Simulating ENSO SSTAs from TAO/TRITON Winds: The Impacts of 20 Years of Buoy Observations in the Pacific Waveguide and Comparison with Reanalysis Products

ANDREW M. CHIODI AND D. E. HARRISON

Joint Institute for the Study of the Ocean and Atmosphere, University of Washington, and NOAA/Pacific Marine Environmental Laboratory, Seattle, Washington

(Manuscript received 7 December 2015, in final form 18 October 2016)

ABSTRACT

The fundamental importance of near-equatorial zonal wind stress in the evolution of the tropical Pacific Ocean's seasonal cycle and El Niño–Southern Oscillation (ENSO) events is well known. It has been two decades since the TAO/TRITON buoy array was deployed, in part to provide accurate surface wind observations across the Pacific waveguide. It is timely to revisit the impact of TAO/TRITON winds on our ability to simulate and thereby understand the evolution of sea surface temperature (SST) in this region. This work shows that forced ocean model simulations of SST anomalies (SSTAs) during the periods with a reasonably high buoy data return rate can reproduce the major elements of SSTA variability during ENSO events using a wind stress field computed from TAO/TRITON observations only. This demonstrates that the buoy array usefully fulfills its waveguide-wind-measurement purpose. Comparison of several reanalysis wind fields commonly used in recent ENSO studies with the TAO/TRITON observations reveals substantial biases in the reanalyses that cause substantial errors in the variability and trends of the reanalysis-forced SST simulations. In particular, the negative trend in ERA-Interim is much larger and the NCEP–NCAR Reanalysis-1 and NCEP–DOE Reanalysis-2 variability much less than seen in the TAO/TRITON wind observations. There are also mean biases. Thus, even with the TAO/TRITON observations available for assimilation into these wind products, there remain oceanically important differences. The reanalyses would be much more useful for ENSO and tropical Pacific climate change study if they would more effectively assimilate the TAO/TRITON observations.

1. Introduction

Zonal winds across the equatorial Pacific exhibit a distinctive behavior characterized by a broad peak in their spectral density of variance in the 3–60-day band, as well as spatially coherent variability across 2°–3° latitude and 10°–15° longitude, for all energetic periods from >2 days to interannual time scales (Harrison and Luther 1990). The Tropical Atmosphere Ocean (TAO) moored buoy array was designed as a minimal observing system capable of resolving these temporal and spatial scales and has proven its effectiveness in allowing us to observe and better quantify the wind stress variability that drives regional upper-ocean circulation and temperature changes during El Niño–Southern Oscillation (ENSO) events. In particular, the TAO and enhanced TAO/Triangle Trans-Ocean Buoy Network (TAO/TRITON) array, which spans the entire tropical Pacific, has been fundamental to improving our understanding of the behavior of subseasonal-timescale wind events that occur over the Pacific oceanic waveguide and are now understood to play an important role in the onset and development of both El Niño and La Niña events.

TAO/TRITON wind observations offer dramatic improvement over what was available prior to the deployment of the buoy array. Attempts at reproducing ENSO sea surface temperature anomaly (SSTA) changes using ocean general circulation models (OGCMs) forced with different pre-TAO wind stress estimates largely revealed a frustrating amount of uncertainty in the wind stress information available then (e.g., Harrison 1989; Harrison et al. 1990). Numerical weather prediction models run in data-assimilating reanalysis mode offer

Denotes Open Access content.

Corresponding author e-mail: Andrew Chiodi, andy.chiodi@noaa.gov

DOI: 10.1175/JCLI-D-15-0865.1

estimates of wind stress at finer spatial scales than are available from the TAO/TRITON data alone. However, there are substantial differences between the commonly used reanalysis fields, and each differs substantially from the estimates based on direct TAO/TRITON observations. For example, near-surface (10 m) wind behavior in the NCEP–NCAR Reanalysis-1 (NCEP) and NCEP–DOE Reanalysis-2 (NCEP2), along with an earlier 40-yr European Centre for Medium-Range Weather Forecasts (ECMWF) Re-Analysis product (ERA-40), was compared to site-matched TAO/TRITON observations in the intertropical convergence zone region by Serra et al. (2007), who found better agreement, in general, for the wind components than wind speed, which suggests that biases in stress may proportionally exceed those of the wind components. Previously, Wittenberg (2004) compared the NCEP wind stress product over the equatorial Pacific with the Florida State University's buoy- and ship-based wind stress estimate (study period 1961–99; Legler and O'Brien 1988) and found weaker zonal stress anomalies in NCEP. Similar deficiencies have been reported for NCEP by Smith et al. (2001) and Auad et al. (2001). Kumar and Hu (2012) examined the regression relationship between zonal equatorial Pacific wind stress and the Niño-3.4 SSTA index among six different reanalysis products and found considerable spread among the associated regression amplitudes, with the result based on NCEP being among the lowest and NCEP2 much closer to the six-reanalysis average. The ongoing effort to redesign the Tropical Pacific Observing System (TPOS) to advance ENSO observation and research in the coming decades has renewed interest in the question of what uncertainty in our knowledge of equatorial Pacific winds means to our ability to observe and better understand ENSO development.

Here, we first examine how well the equatorial Pacific zonal wind stress fields available from three widely used numerical weather prediction model reanalyses compare with the estimates available from direct TAO/TRITON buoy wind observations. Then we examine how well ENSO SSTA conditions can be reproduced in an OGCM from the available knowledge of zonal equatorial Pacific wind stress, which permits a complementary–independent evaluation of wind stress product fidelity. The reanalyses used here include first-generation (NCEP), second-generation (NCEP2), and recent-generation (ERA-Interim, as well as TropFlux) products that have been used in the recent efforts to understand the ENSO SSTA behavior observed in 2014/15 (Menkes et al. 2014; Chen et al. 2015; Min et al. 2015). We use up-to-date TAO/TRITON observations, the reanalysis products, and an ocean model known to reproduce observed upper-ocean current and temperature variability in a usefully accurate manner when forced with accurate wind stress information (Harrison and Chiodi 2009; Harrison et al. 2009; Chiodi et al. 2014; Chiodi and Harrison 2015). We begin with continually wind-forced ocean model integrations (referred to as hindcasts hereafter) that are forced by TAO/TRITON wind observations alone and next look at site-matched comparison statistics between TAO/TRITON-estimated zonal wind stress and the reanalysis products for each year from 1986 to 2014. We also systematically examine how well each wind stress dataset is able to reproduce observed end-of-year [October–December (OND)] ENSO SSTA conditions when used to force our OGCM. We consider model runs and wind stress integrations over the subset of years for which wind observations are available from the majority (>60% coverage) of the TAO/TRITON buoys along the equator. We have generally found poor hindcast results in years with TAO/TRITON coverage below this level (a case study of 2014/15 has been submitted to this journal). This criterion (at least 60% TAO/TRITON coverage in the waveguide) identifies the 20 years from 1992 to 2011 as the subset for hindcast study (leaving out the deployment period from the mid-1980s to mid-1990s, along with the recent array collapse in 2012–14).

2. Data and methods

For SST information, we use the NOAA Optimum Interpolation SST (OISST) product, version 2 (NOAA 2002), described by Reynolds et al. (2002) and provided by the NOAA/Oceanic and Atmospheric Research/Earth System Research Laboratory Physical Sciences Division (Boulder, Colorado).

We use daily average wind observations from the TAO/TRITON (TAO Project Office 2000) moored buoy array, described by McPhaden et al. (2010) and made available by the NOAA/Pacific Marine Environmental Laboratory TAO Project Office, to estimate wind stress. The TAO/TRITON daily average wind speeds are calculated from 10-min averages (P. Freitag 2015, personal communication) and available from the TAO website (TAO Project Office 2000). The wind data are converted to zonal pseudostress using the following formula:

$$\tau^x = \rho_a C_d |\mathbf{U}| u,$$

with air density ρ_a assigned the value of 1.25 kg m^{-3}, $C_d = 1.3 \times 10^{-3}$. The $\mathbf{U}$ is the 10-m wind vector and u its zonal component. This same formula for TAO-based pseudostress was also used by Harrison and Chiodi (2009). Wind stress is given here in SI units of pascal (1 Pa = 1 N m^{-2}). Daily average TAO/TRITON wind stress anomalies at each buoy are calculated by

subtracting the daily wind stress climatology determined based on linear interpolation of the monthly averaged seasonal cycle, which is calculated using all wind observations available during the 1986–2014 study period.

It bears noting that when sufficient meteorological observations are available, TAO/TRITON-based wind stress estimates calculated based on the COARE 3.0b parameterization (Fairall et al. 2003; Cronin et al. 2006) are also made available by the TAO Project Office (www.pmel.noaa.gov/tao/oceansites/flux/main.html). We have compared model simulations forced with the momentum fluxes calculated based on each of these two approaches and found similar results (e.g., 2002 weekly average Niño-3.4 rms difference < 0.1°C) when the two momentum flux estimates are applied with the same data gaps. There are, however, more gaps in the COARE case (e.g., ~25% more in 2002), and a more accurate SSTA simulation results from forcing with all available pseudostress estimates. For this reason, although we expect wind stress calculated from TAO/TRITON observations and the COARE 3.0b parameterization to also provide accurate wind stress information when available, we herein rely on TAO/TRITON wind observations and the formula listed above for zonal wind stress information.

To force the ocean model in our base-case experiments, we form an estimate of the wind stress anomaly field along the equatorial Pacific using just the daily averaged TAO/TRITON wind observations. Since it is the zonal wind stresses closest to the equator that most efficiently drive equatorially trapped oceanic Kelvin waves, we do this in a manner that maximizes the use of the available near-equatorial buoy observations. We also take advantage of the fact that the buoy spacing was designed to match the observed covariance length scale of the wind variability. The procedure is as follows: The zonal length of the basin is first divided into subregions surrounding each (north–south) buoy line, with east–west boundaries specified equidistant from the buoy-line longitudes, and north–south boundaries at 5°S and 5°N. The respective 2°S–2°N average (core waveguide) buoy wind stress anomalies are then applied to each buoy region with tapering to zero poleward of 5° at an *e*-folding scale of 0.5°. This step of averaging over the core waveguide can be thought of as a means of filling the gap caused by a core-waveguide buoy dropout, based on the other, still available, core-waveguide observations. No zonal smoothing is applied. Anomalies are applied for each day with observations available from at least one of the three possible near-equatorial buoys, and zero anomaly is applied on days without observations in the core of the waveguide.

The meridional-direction (*y* direction) averaging step described above constitutes the main difference from the simplest approach to synthesizing a wind field based on buoy observations that we could think of, which is drawing equidistant boxes around each buoy site (including in the *y* direction) and filling the buoy boxes with the respective buoy winds (or zero anomaly if the buoy measurements are unavailable). We have also rerun our model integrations with this alternative "TAO box" wind stress field. Doing this yields model results that are qualitatively equivalent and quantitatively very similar to the base-case ones presented below (e.g., end-of-year Niño-3.4 model–observation correlations within 1% of one another), although marginally better accuracy is seen on average in the base case. For example, the end-of-year Niño-3.4 rmse is improved by 0.05°C in the base case relative to the TAO box. This small improvement is consistent with the proposition that, because equatorial Pacific winds have a meridional covariance length scale of 2°–3°, observations within 2° latitude of the equator often provide useful estimates for conditions at the equator even in cases where the 0° buoy is not reporting. In other words, *y* averaging over 2°S–2°N in the base case provides a useful (if small) improvement over the TAO-box results because it usefully fills gaps caused by buoy dropouts in the heart of the waveguide with information from nearby observations. The conclusions reached herein, however, do not depend on performing this *y*-averaging procedure.

We also use surface wind stress estimates from three numerical weather models run in data assimilation mode. These are the NCEP–NCAR Reanalysis-1 (NCEP 1996) described by Kalnay et al. (1996), the NCEP–DOE Reanalysis-2 (NCEP 2002) described by Kanamitsu et al. (2002), and the ECMWF interim reanalysis (ERA-Interim, hereafter ERA-I; ECMWF 2011) described by Dee et al. (2011). Each reanalysis assimilates TAO/TRITON observations. ERA-I also assimilates satellite-based estimates of near-surface wind variability, including those from the *ERS-1* and *ERS-2* scatterometers and QuikSCAT, which span the 1992–2010 period in a piecewise manner. In the cases of NCEP and NCEP2, we use the daily average wind stresses provided by the project websites on a 2.5° latitude × 2.5° longitude grid and interpolate to the nominal TAO/TRITON sites when calculating the buoy–reanalysis comparison statistics. A second set of results (not shown for brevity) in which no interpolation was performed and the NCEP and NCEP2 data from the reanalysis grid box centered nearest the respective buoy location were used produces quantitatively similar results. In the ERA-I case, daily averaged wind stress was calculated from the available 3-h averages and downloaded at 1° × 1° resolution such that the grid boxes are already centered on the nominal buoy locations; data from the grid box containing the buoy location were used in this case.

Additionally, we have repeated the buoy comparisons and ocean model runs described below using the TropFlux (National Institute of Oceanography and IPSL 2012) wind stresses, which are based on the near-surface winds from ERA-I but use a bulk algorithm developed for use in the tropics, along with adjustments for factors such as wind gustiness to estimate tropical wind stress. TropFlux wind stress estimates have been shown to offer small but consistent improvements over ERA-I, evaluated against the available tropical moored buoy information, including TAO/TRITON (Praveen Kumar et al. 2013). The ERA-I dataset, nonetheless, remains popular. We find in our analyses that the TropFlux-based results are generally very similar to their ERA-I counterparts; the ERA-I- and TropFlux-forced ocean model simulations (described below) yield results that differ by only a few percent from one another in terms of their rms difference and correlation with the observed end-of-year Niño-3.4 SSTA conditions. Because these differences are small for our purposes, we present only the ERA-I set of results herein.

In addition to reanalyses like ERA-I, which include satellite-based near-surface winds along with in situ observations, there are other products currently available that combine the satellite and reanalysis winds (along with in situ observations in some cases) in a manner that places greater emphasis on the satellite-based data (e.g., Zhang et al. 2006; Atlas et al. 2011). Our experience with the NOAA Blended Sea Winds product (Zhang et al. 2006) suggests that the product's accuracy largely depends on which satellites are available during the period–year in question (this product is included in our 2014/15 study mentioned above). We believe that it is important to try and better understand the current satellite wind situation by examining ocean model simulations forced by winds from the individual missions alone (e.g., the currently available ASCAT A and B scatterometer data, which begin near the end of our study period, in May 2007 and September 2012, respectively), but this research is beyond the scope of the present study.

The OGCM we use is derived from the Philander and Siegel (1985) version of the Bryan–Semtner–Cox (Bryan 1969; Semtner 1974; Cox 1984) primitive equation model, and the configuration used here is based on NOAA's Geophysical Fluid Dynamics Laboratory (GFDL) Modular Ocean Model, version 4 (MOM4; Griffies et al. 2003). The global version of MOM4 is the oceanic component of the GFDL Climate Model, version 2 (CM2.0; Gnanadesikan et al. 2006). It is used here with the surface solar heat flux parameterization described by Harrison (1991). We employ it with 27 levels in the vertical, 17 of which are above 250 m. The upper grid point is at 5 m, with a uniform 10-m grid in the upper 100 m and an increasingly nonuniform grid deeper. The horizontal grid is uniform between 10°N and 10°S, with 0.33° resolution in latitude and 1.0° resolution in longitude. Poleward of 10°, the meridional resolution increases nonuniformly, to 50°N and to 25°S. The model experiments described here begin from a ''spun up'' state reached by applying over several years the climatological wind stress and surface heat flux parameterization of Harrison et al. (2009). The spin-up mode (but not experiment mode) surface heat flux parameterization includes the specification of observed 2-m air temperature during calculation of latent and sensible heat fluxes, which acts to constrain SST drift during the spin-up years, while keeping the applied surface heat fluxes consistent with the observed climatology to within the associated uncertainty (Harrison et al. 2009). The model experiments thereby start from a base state that rather accurately reproduces the main features of the observed climatological surface and upper-ocean subsurface currents and thermal structure, including the zonal gradient in equatorial SST (as documented in Harrison et al. 2009). The climatological wind stress used in the spin up was developed from the COADS marine dataset and Large and Pond (1981) stability-dependent drag coefficient by Harrison (1989). Our experimental procedure is similar to that of Harrison and Chiodi (2009) and was used more recently by Chiodi et al. (2014) and Chiodi and Harrison (2015). In the experiment mode, the longwave (set to constant of 55 $W m^{-2}$) and shortwave fluxes [based on model SSTs and specified constants; see Harrison (1991) and Harrison et al. (2009)] are specified as in the spin up, but latent and sensible heat fluxes are determined differently, according to the Philander and Siegel (1985) scheme, based on the applied wind speed (including wind speed anomalies commensurate to the wind stress anomalies applied in the experiment case) and a constant sea surface–2-m air temperature difference of 1°C (for sensible heat flux) and constant near-surface relative humidity of 0.8 (for latent heat flux). These constants are representative of the average conditions over tropical oceans. It bears noting that the model SST is not constrained by observed air or surface temperature during the experiments. The driving force behind the SSTAs that appear in this experimental configuration is the wind variability, and particularly its expression in zonal wind stress anomalies (e.g., wind speed increases associated with a westerly wind event will lead to some offsetting local increases in the upward latent heat flux, but it is the ocean circulation changes driven by the applied momentum flux that warm the oceanic waveguide in this case and dominate the model response). In our base-case experiment, zonal wind stress anomalies

calculated from the TAO/TRITON wind observations are horizontally interpolated to the ocean model grid and added to the climatological zonal momentum flux that was used in the spin up. The SSTAs are then calculated based on the difference between runs with (the experiment) and without (the control) the applied zonal wind stress anomalies.

3. TAO/TRITON hindcasts

Here, we show that an appropriate ocean model, forced from TAO/TRITON wind observations on their own, can often provide a useful simulation of the observed development of equatorial Pacific SSTAs during ENSO events. We take as case examples the El Niño years of 2002 and 1997. These years are among those that exhibited some of the warmest equatorial Pacific anomalies in the study period (e.g., maximum observed monthly averaged Niño-3.4 values of +1.6° and +2.7°C, respectively). They are also among those in which the model does well in simulating the detailed development of equatorial Pacific SSTAs; because of limitations of the model and surface forcing, smaller-amplitude events are typically simulated less successfully. The loss of multiple buoys adjacent to one another, especially if during major wind events, can also impair our knowledge of the winds and ability to simulate SSTAs in some years more than others. Results from all 20 hindcast years are nonetheless included in the statistics discussed in section 5.

Figure 1 shows the equatorial Pacific SSTA development simulated in our OGCM when it is forced with a wind stress field estimated from the TAO/TRITON wind observations collected in 2002. TAO/TRITON observational coverage in this year was relatively good, reaching ~85% data return along the equator. Although the model run starts from climatological mean conditions (zero anomaly at the beginning of 2002) and is forced using the available TAO/TRITON wind observations alone, the model reproduces a qualitatively correct SSTA development. The basic structure of the observed and modeled SSTA patterns agree, and although the model lacks some midyear warming in the Niño-3.4 region compared to the observations (model and observed Niño-3.4 values are shown in Fig. 1, right), the end-of-year Niño-3.4 values are correct. The TAO/TRITON-observed zonal wind anomalies clearly provide a dominant forcing for the evolution of SSTAs in this event.

We have hindcast the large El Niño event of 1997 in the same manner and found similar results (Fig. 2). The basic equatorial SSTA pattern development is again well reproduced by the model in the 1997 case. However, differences in details exist; the model first warms the cold tongue too quickly during the spring then not quickly enough in the late summer–fall (the loss of some buoys along the equator during this major event reduced the accuracy of the buoy-based stress estimates during the latter period). Nonetheless, the model does well at reproducing the basic pattern and amplitudes of the observed SSTA development, and the model again produces an accurate December Niño-3.4 value. The TAO/TRITON wind observations clearly provide a useful basis for simulating the observed SSTA behavior in both the strong 1997 El Niño event and the more moderate 2002 event.

The value of having accurate knowledge of wind anomalies over the western tropical Pacific (i.e., where the TRITON buoys are located) as well as farther east (the TAO part of the array) can also be demonstrated. When the wind stress anomalies west of the date line (180°) are omitted from the 2002 hindcast shown in Fig. 1, the development of warm SSTAs in the model occurs much too late (the model Niño-3.4 remains very near 0°C through August, when the observations have reached ~+1°C) and with insufficient amplitude, reaching an end-of-year Niño-3.4 value of only ~0.6°C, which is almost 1°C lower than the observed value (Fig. 3). Losing knowledge of wind stress anomalies over the western Pacific means losing about half of the signal in this case. Losing the eastern half (experiment not shown for brevity) also degrades the hindcast fidelity to a comparable degree. Our particular interest here in the role of the western Pacific wind stress is motivated by the fact that the TRITON part of the array is currently scheduled to go out of service, and the observing system's ability to provide accurate knowledge of wind variability without any buoy observations (e.g., through reanalyses or satellite wind products produced without access to the buoy observations) is currently unknown. Other case studies indicate similar loss of ability to simulate SSTAs usefully with part of the array omitted.

4. Wind stress comparison

a. Statistical comparison of daily averaged wind stress

We look first at how well daily averaged wind stress from ERA-I, NCEP, and NCEP2 compares with daily averaged wind stress estimated from the available TAO/TRITON wind observations. Our comparison is based on daily averaged reanalysis data, subsampled at the available buoy days–sites. Our focus is on the near-equatorial longitudes (2°S–2°N), where wind stress changes are most effective in driving waveguide circulation changes (e.g., equatorially trapped Kelvin waves).

The correlation, rms difference, and mean offset between daily averaged wind stress from TAO/TRITON and each of the three reanalysis products are listed in

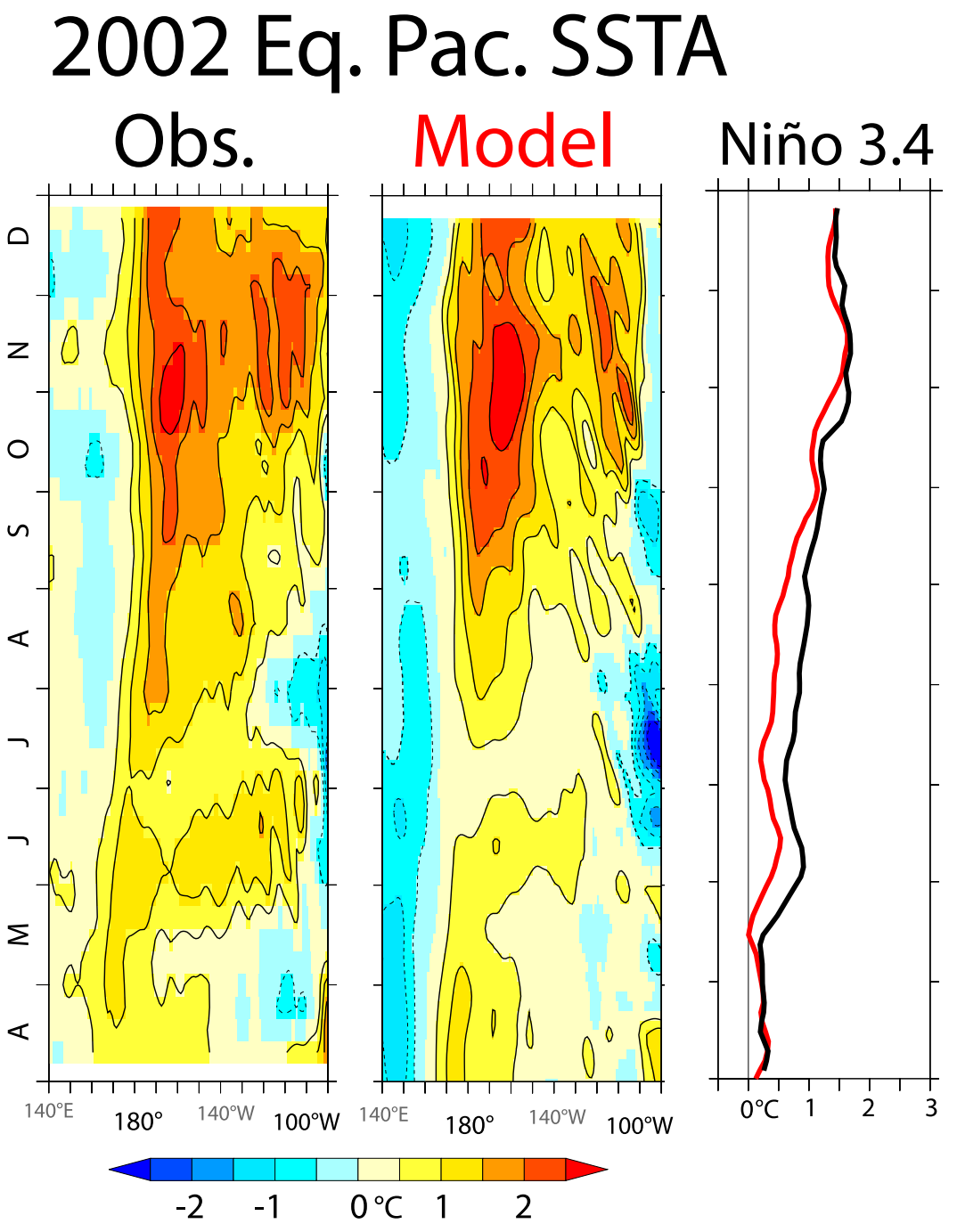

FIG. 1. Equatorial (2°S–2°N averaged) April to December Pacific SSTAs based on (left) the NOAA OISST dataset and (center) an ocean model forced with pseudostress estimated from the available 2002 TAO/TRITON buoy wind observations. (right) The respective SSTAs averaged over the Niño-3.4 region.

Tables 1–3, along with the total number of TAO/TRITON-based daily averages available at the given location in the 1986–2014 period. The distribution of observations by year is shown in Fig. 4.

Some common features emerge in these statistics. In each case, correlation between the respective numerical weather reanalysis data and TAO/TRITON is higher over the western than eastern part of the basin. This may be because interannual time-scale changes in the wind are more pronounced in the western than eastern equatorial Pacific zonal wind (Harrison and Luther 1990) and perhaps are more easily resolved by the reanalyses than

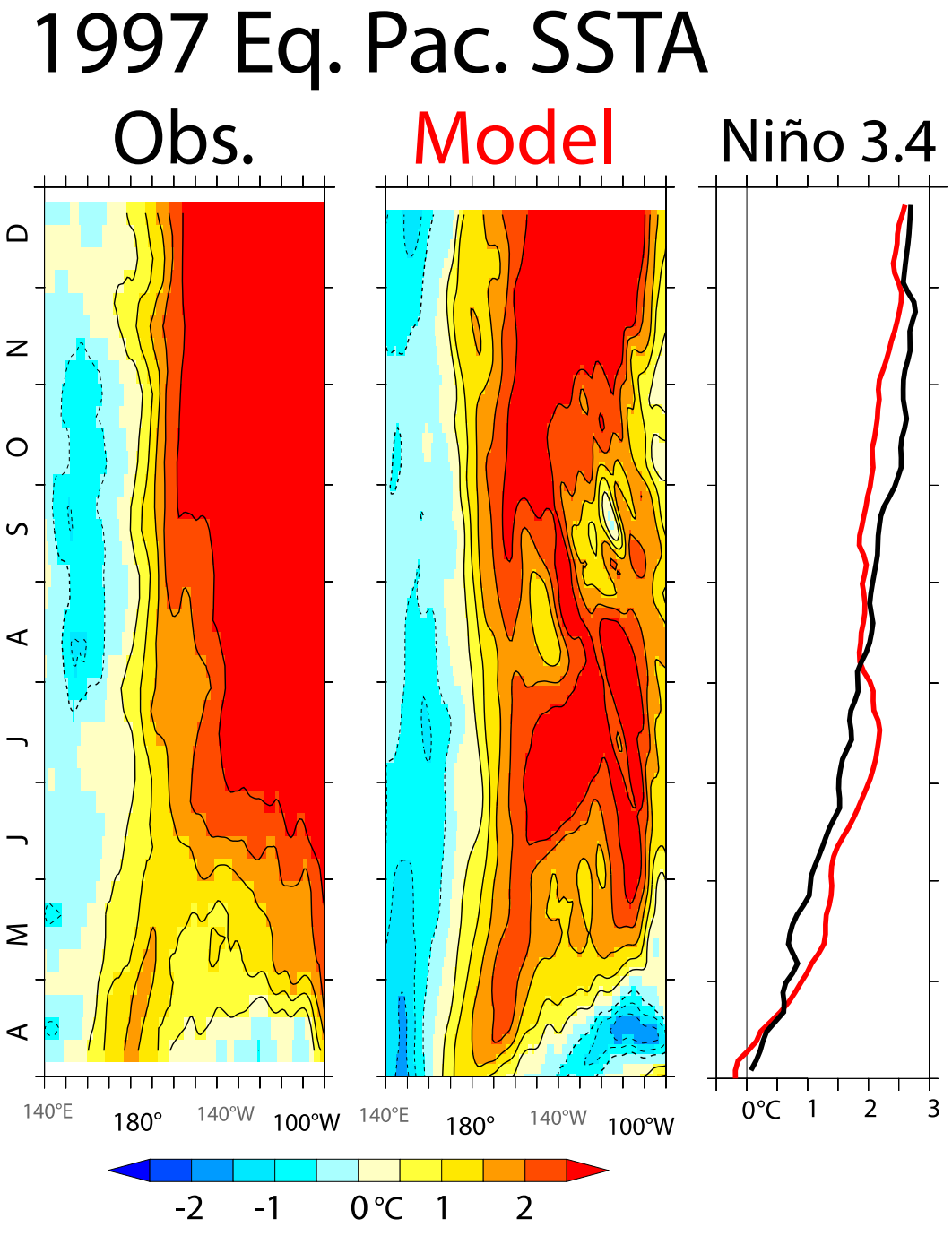

FIG. 2. As in Fig. 1, but for 1997.

other types of variability. On the other hand, the rms differences between the reanalyses and TAO/TRITON are generally largest in the heart of the equatorial easterly trade wind regime (eastern-central Pacific) where the zonal winds are strongest. It is here that even seemingly small increases in wind speed, such as those associated with the equatorial Pacific easterly wind surges, produce substantial wind stress increases because of the nonlinear relationship between wind speed and stress (e.g., Large and Pond 1981; Chiodi and Harrison 2015). Because of this, it is especially difficult to accurately estimate the zonal wind stress changes that occur in the eastern-central Pacific.

Overall, it is ERA-I that provides the closer match to TAO/TRITON. The average rms difference

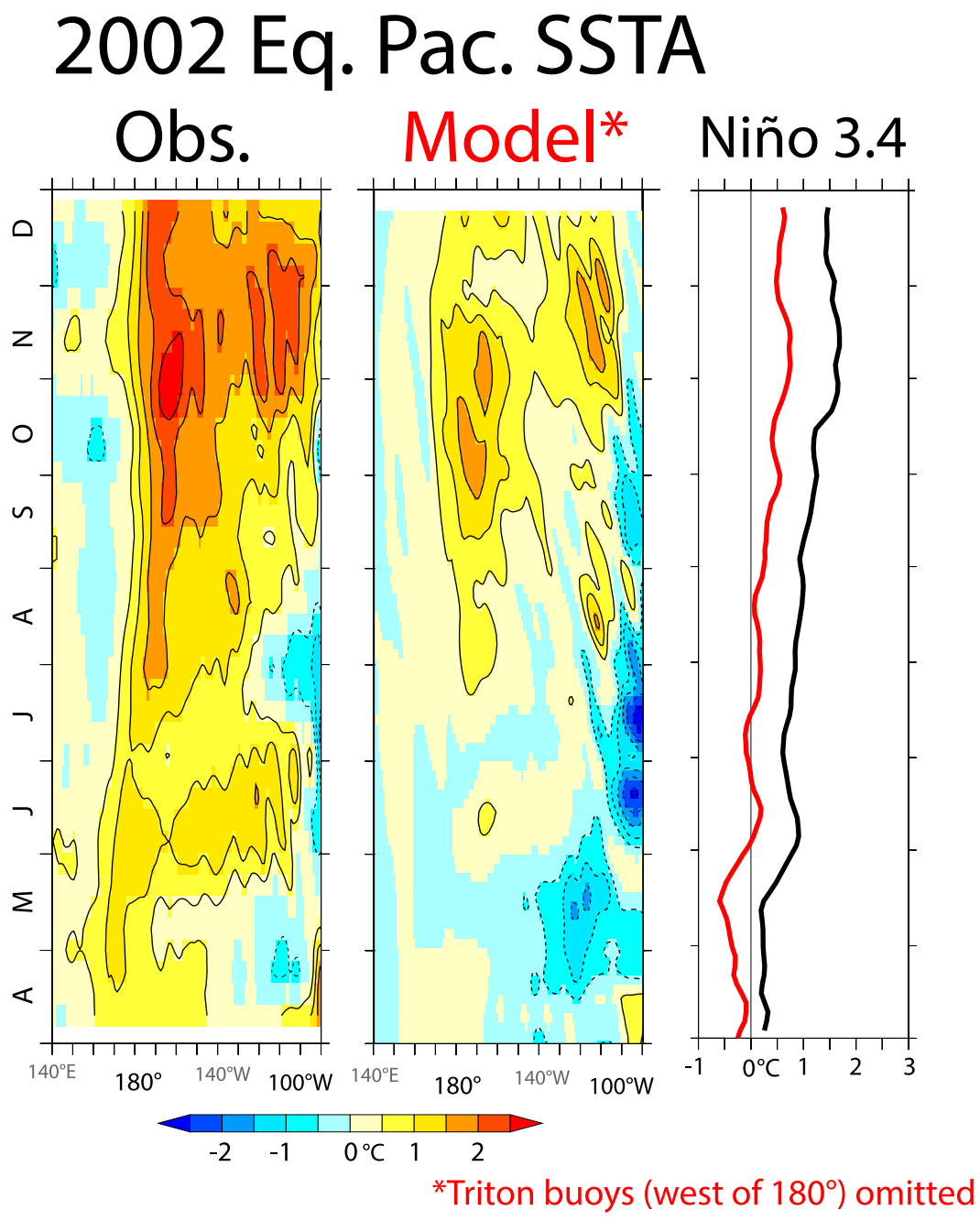

FIG. 3. As in Fig. 1, but for climatological wind stress (zero anomaly) applied west of 180° longitude.

(correlation) between TAO/TRITON and ERA-I is 0.017 Pa (0.89), which is noticeably better than the NCEP and NCEP2 reanalysis products, which yield rms differences (correlations) of 0.024 Pa (0.73) and 0.023 Pa (0.70), respectively. Substituting TropFlux for ERA-I in this case confirms the Praveen Kumar et al. (2013) finding that TropFlux offers small improvements over ERA-I in terms of its closeness to TAO/TRITON observations. Since these improvements remain small for our purposes (as discussed above), we present just the ERA-I results.

Although ERA-I (and TropFlux) tends to match TAO/TRITON more closely than NCEP or NCEP2, the discrepancies between ERA-I (and TropFlux) and the buoy observations are still substantial. For example, Fig. 5 illustrates the fact that the ERA-I data still yield an rms difference (based on daily averages) that remains a sizeable fraction (~40%) of the total TAO/TRITON-averaged

TABLE 1. Statistical comparison of daily average wind stress estimates based on TAO/TRITON buoy measurements and ERA-I stresses, subsampled at the times/locations for which buoy observations are available. Buoy lines are at (top) 2°N, (middle) 0°, and (bottom) 2°S. Rows in each subtable are as follows: 1) Buoy latitude and longitude, 2) correlation r between buoy and reanalysis daily averaged wind stress, 3) rms difference (rmsd) between buoy and reanalysis daily averaged wind stress, 4) all-day-averaged reanalysis wind stress (mean), 5) all-day-averaged wind stress bias (Δ; reanalysis minus buoy), and 6) number of daily averages available from TAO/TRITON at the given location in the 1986–2014 study period (No. obs).

2°N	137°E	147°E	156°E	165°E	180°	170°W	155°W	140°W	125°W	110°W	95°W
r	0.94	0.90	0.94	0.92	0.94	0.91	0.90	0.89	0.87	0.83	0.81
Rmsd	0.016	0.017	0.015	0.018	0.017	0.018	0.018	0.016	0.015	0.015	0.011
Mean	0.003	−0.005	−0.014	−0.027	−0.055	−0.063	−0.071	−0.066	−0.054	−0.034	−0.007
Δ	0.002	−0.004	−0.006	−0.007	−0.011	−0.008	−0.010	−0.004	−0.003	0.001	0.004
No. obs	3445	4806	6057	8046	6268	5878	7553	8482	6874	8107	4241

0°N	137°E	147°E	156°E	165°E	180°	170°W	155°W	140°W	125°W	110°W	95°W
r	—	0.95	0.95	0.94	0.95	0.94	0.91	0.88	0.82	0.81	0.81
Rmsd	—	0.013	0.013	0.015	0.015	0.016	0.021	0.020	0.022	0.017	0.010
Mean	—	−0.007	−0.010	−0.020	−0.049	−0.060	−0.069	−0.070	−0.057	−0.040	−0.015
Δ	—	−0.003	−0.004	−0.005	−0.008	−0.008	−0.014	−0.013	−0.015	−0.010	0.001
No. obs	41	4991	6422	7344	6214	8995	7207	9417	7516	8005	4726

2°S	137°E	147°E	156°E	165°E	180°	170°W	155°W	140°W	125°W	110°W	95°W
r	—	—	0.94	0.94	0.95	0.94	0.92	0.89	0.87	0.87	0.85
Rmsd	—	—	0.014	0.016	0.015	0.017	0.019	0.022	0.021	0.015	0.010
Mean	—	—	−0.003	−0.014	−0.047	−0.060	−0.074	−0.077	−0.066	−0.050	−0.026
Δ	—	—	−0.003	−0.004	−0.008	−0.009	−0.012	−0.015	−0.014	−0.008	−0.002
No. obs	0	0	6643	6986	7569	6906	7008	8617	7175	7411	5064

wind stress acting over the equatorial Pacific during this period.

Figure 6 provides an example of how well daily averaged wind stress from ERA-I, NCEP, NCEP2, and TAO/TRITON compares over a single year (2002) at a single buoy site (0°, 180°). In this case, the TAO/TRITON data reveal several easterly and westerly wind events with time scales of roughly one week (e.g., the easterly event

TABLE 2. As in Table 1, but for the NCEP reanalysis.

2°N	137°E	147°E	156°E	165°E	180°	170°W	155°W	140°W	125°W	110°W	95°W
r	0.86	0.80	0.83	0.79	0.81	0.77	0.75	0.72	0.72	0.68	0.68
Rmsd	0.016	0.018	0.020	0.024	0.023	0.028	0.028	0.034	0.032	0.028	0.014
Mean	−0.001	−0.004	−0.007	−0.016	−0.037	−0.041	−0.043	−0.037	−0.027	−0.016	−0.005
Δ	−0.003	−0.002	0.004	0.00	0.008	0.014	0.018	0.026	0.025	0.020	0.007
No. obs	3445	4806	6057	8046	6268	5878	7553	8482	6874	8107	4241

0°N	137°E	147°E	156°E	165°E	180°	170°W	155°W	140°W	125°W	110°W	95°W
r	—	0.86	0.85	0.83	0.83	0.79	0.78	0.70	0.67	0.65	0.67
Rmsd	—	0.017	0.019	0.025	0.023	0.027	0.025	0.028	0.023	0.020	0.014
Mean	—	−0.006	−0.004	−0.011	−0.033	−0.037	−0.041	−0.038	−0.028	−0.019	−0.01
Δ	—	−0.002	0.002	0.004	0.009	0.016	0.015	0.019	0.015	0.011	0.007
No. obs	41	4991	6422	7344	6214	8995	7207	9417	7516	8005	4726

2°S	137°E	147°E	156°E	165°E	180°	170°W	155°W	140°W	125°W	110°W	95°W
r	—	—	0.87	0.80	0.85	0.81	0.81	0.71	0.74	0.66	0.71
Rmsd	—	—	0.019	0.025	0.023	0.025	0.029	0.030	0.028	0.025	0.015
Mean	—	—	−0.001	−0.008	−0.031	−0.037	−0.041	−0.039	−0.032	−0.025	−0.014
Δ	—	—	−0.001	0.003	0.009	0.013	0.021	0.022	0.021	0.017	0.009
No. obs	0	0	6643	6986	7569	6906	7008	8617	7175	7411	5064

TABLE 3. As in Table 1, but for the NCEP2 reanalysis.

2°N	137°E	147°E	156°E	165°E	180°	170°W	155°W	140°W	125°W	110°W	95°W
r	0.79	0.77	0.79	0.72	0.76	0.71	0.68	0.58	0.59	0.62	0.60
Rmsd	0.020	0.020	0.021	0.027	0.025	0.030	0.028	0.032	0.028	0.023	0.015
Mean	-3×10^{-4}	−0.003	−0.009	−0.020	−0.037	−0.043	−0.047	−0.047	−0.037	−0.025	−0.009
Δ	−0.003	−0.002	4×10^{-4}	4×10^{-4}	0.008	0.012	0.014	0.015	0.015	0.011	0.002
No. obs	3445	4806	6057	8046	6268	5878	7553	8482	6874	8107	4241

0°N	137°E	147°E	156°E	165°E	180°	170°W	155°W	140°W	125°W	110°W	95°W
r	—	0.86	0.82	0.76	0.82	0.77	0.75	0.64	0.66	0.65	0.61
Rmsd	—	0.016	0.019	0.026	0.022	0.025	0.024	0.025	0.019	0.017	0.014
Mean	—	−0.007	−0.007	−0.015	−0.035	−0.042	−0.044	−0.047	−0.036	−0.028	−0.015
Δ	—	−0.003	1×10^{-4}	1×10^{-4}	0.007	0.011	0.012	0.010	0.006	0.003	0.002
No. obs	41	4991	6422	7344	6214	8995	7207	9417	7516	8005	4726

2°S	137°E	147°E	156°E	165°E	180°	170°W	155°W	140°W	125°W	110°W	95°W
r	—	—	0.84	0.74	0.83	0.79	0.78	0.67	0.72	0.68	0.66
Rmsd	—	—	0.019	0.027	0.022	0.023	0.025	0.025	0.022	0.019	0.013
Mean	—	—	−0.003	−0.013	−0.035	−0.043	−0.047	−0.049	−0.041	−0.034	−0.021
Δ	—	—	−0.002	−0.002	0.005	0.008	0.015	0.012	0.012	0.008	0.003
No. obs	0	0	6643	6986	7569	6906	7008	8617	7157	7411	5064

in June). It is clear that NCEP and NCEP2 substantially underrepresent the amplitude of these events (especially the two westerly events in December). ERA-I, on the other hand, appears to resolve these events and generally tracks TAO/TRITON more closely than the other two reanalysis products, which is consistent with it having the lower rms difference. But there are still substantial discrepancies between ERA-I and TAO/TRITON. This becomes clearer in Fig. 6 (bottom), where these same four time series are overlaid after they have been filtered with a 30-day running-mean boxcar average. During several months,

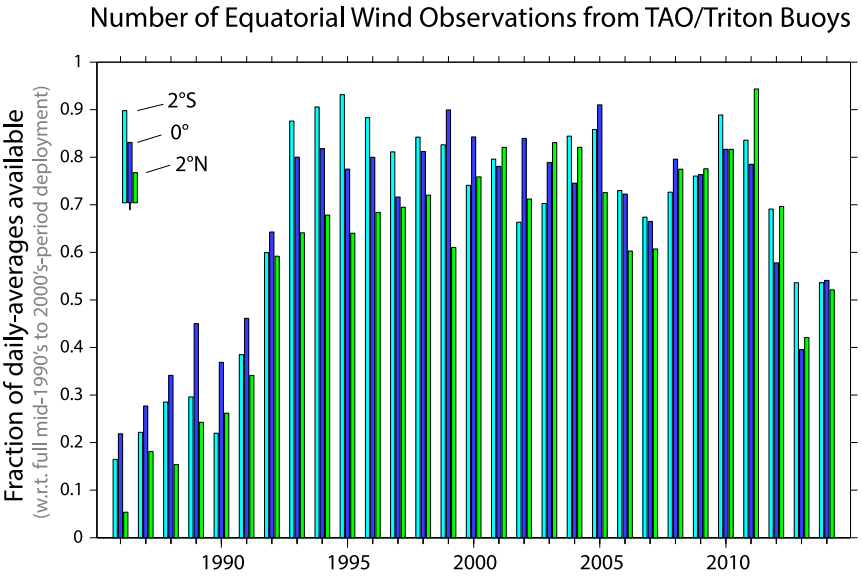

FIG. 4. Number of daily averaged wind observations available from the TAO/TRITON buoy array per year for 1986–2014. The number is expressed as the fraction of the total number of daily averages possible based on full data return from the completely deployed array [i.e., the 11 buoys spanning 137°E–95°W along 2°N (green), the 10 buoys spanning 147°E–95°W along 0° (blue), and the 9 buoys spanning 156°E–95°W along 2°S, cyan)].

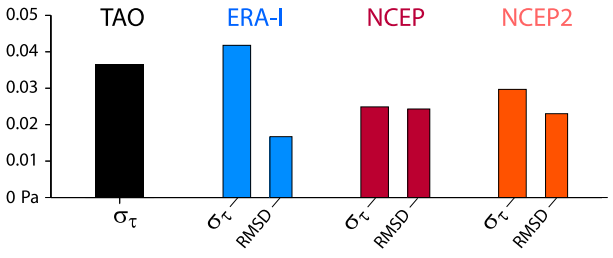

FIG. 5. Mean wind stress standard deviation (σ_τ) based on daily averaged TAO/TRITON buoy observations made over the equatorial (2°S–2°N) Pacific for 1986–2014. The reanalysis data have been subsampled at the times and locations of the available buoy observations. The bars to the right of each of the reanalysis results indicate the rms difference between TAO and the respective reanalysis data.

including the times of the easterly events, it is evident that the net wind stress is more easterly in ERA-I than TAO/TRITON. This is consistent with our previous finding that ERA-I often overestimates easterly wind surge amplitudes, relative to the buoy observations, during this study period (Chiodi and Harrison 2015).

b. *Year-to-year variations in wind stress*

The net amount of wind stress applied to the equatorial Pacific is a key forcing for ENSO SSTA conditions. In this section, we compare annual (January through December) averages of equatorial Pacific wind stress based on each dataset. In each reanalysis case (ERA-I, NCEP, and NCEP2), the wind stress integrals are based on the estimates sampled at the times/locations of the available buoy wind observations. Results are shown for TAO/TRITON and each (buoy sampled) reanalysis product in Fig. 7.

Compared to TAO/TRITON, the ERA-I field overestimates the net (easterly) wind stress acting on the equatorial Pacific each year, whereas NCEP underestimates the net equatorial Pacific wind stress. Wittenberg (2004) has previously found that NCEP underestimates this quantity relative to the observation-based Florida State University (FSU) winds considered over a previous period (cf. Auad et al. 2001). We find that NCEP2 also underestimates annual mean wind stress, relative to TAO/TRITON, in the vast majority of the 29 years considered here, and by an average of 33% (Fig. 7). The spread in total wind stress among these four datasets is a large fraction of their mean (50% based on average range and TAO/TRITON mean). In particular, the NCEP- and ERA-I-based estimates of net wind stress acting over the equatorial Pacific differ greatly (by about factor of 2) with TAO/TRITON estimates falling between these two.

Accurate knowledge of the long-term average (often referred to as "base state") wind stress acting over the equatorial Pacific is a key aspect of the region's ocean–atmosphere coupling and an important benchmark for efforts attempting to accurately simulate this system in coupled models, such as those described in the IPCC's Fifth Assessment Report (Flato et al. 2013). Nonetheless, when diagnosing ENSO SSTA development is the goal, we often focus on deviations from the base state. Correspondingly, Fig. 8 shows what happens after the annual averages from Fig. 7 have been demeaned such that each 29-yr time series sums up to zero. From Fig. 8, it is clear that the reanalysis estimates tend to agree with TAO/TRITON in regards to which years have positive/negative wind stress anomaly peaks. It is also clear, however, that the peak amplitudes differ in character from one dataset to another. NCEP and NCEP2 both tend to estimate smaller-amplitude interannual peaks than TAO/TRITON (by 32% and 26%, respectively, based on the standard deviation of time series plotted in Fig. 8). ERA-I, on the other hand, has many peaks with larger amplitudes than TAO/TRITON (e.g., the warm-ENSO-SSTA years of the early 1990s and recent La Niña years, like 2010/11). Closer inspection of the differences between TAO/TRITON and ERA-I (shown in Fig. 8, bottom), however, reveals a trend-ike temporal pattern over this period, indicative of the fact that ERA-I has estimated a more easterly wind stress than TAO/TRITON in each year since 2004 (with the largest easterly deviations in 2010 and 2011) and a more westerly wind stress than TAO in most all of the years prior to this date (with the largest westerly offsets in the early 1990s).

It deserves mention that the trend in the equatorial Pacific zonal wind over the last 20 to 30 years, including its depiction in the ERA-I product, has been the subject of a great deal of attention recently (e.g., England et al. 2014). We find that the magnitude of the trend calculated over recent decades (or similarly, the change in mean wind stress between the first and second half of the study period) depends greatly on which dataset is used to quantify it. Particularly, the 1986–2014 linear trend (i.e., slope of the best-fit line) in mean equatorial Pacific wind stress based on the available TAO/TRITON winds (-1.42×10^{-5} Pa yr^{-1}) differs by about a factor of 20 from its ERA-I (site matched) counterpart (-2.66×10^{-4} Pa yr^{-1}). If just the 20 years that meet the >60% coverage criteria are used instead (1992–2011), in both cases, the linear-trend slope magnitude increases since this is now a shorter period that begins (ends) with an El Niño (La Niña) year, but the slope in ERA-I (-9.35×10^{-4} Pa yr^{-1}) remains about a factor of 2 greater than

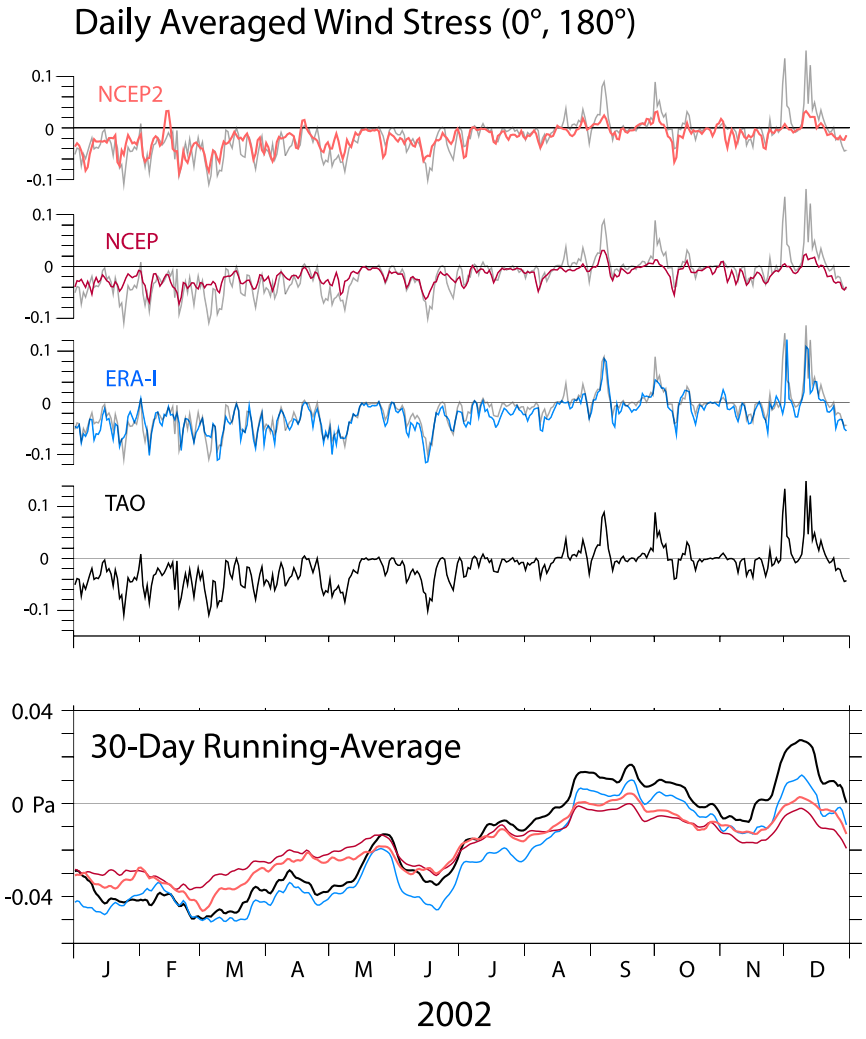

FIG. 6. (top) Daily averaged wind stress estimated at 0° latitude, 180° longitude based on NCEP (red), NCEP2 (purple), ERA-I (blue), and the TAO buoy measurements (black). (bottom) The 30-day running means of these four time series.

TAO/TRITON (-5.17×10^{-4} Pa yr^{-1}). Similarly, the change in ERA-I wind stress between the second (2002–11) and first (1992–2001) 10 years of the 1992–2011 period (-0.0068 Pa) is about twice that seen in the TAO/TRITON observations (-0.0032 Pa). The ERA-I trend–decadal change over this study period appears to be clearly too large. The oceanic implications of the spurious decadal-scale biases in ERA-I will be discussed in section 5.

A reviewer's comment has motivated us to mention that, for ENSO, trends such as these, which are observed only over multidecadal periods, should not be considered representative of longer-term trend behavior or expected to continue over the coming decades (Wittenberg 2009; Stevenson et al. 2010; Harrison and Chiodi 2015).

In summary, the results described in this section have shown that, of the reanalysis products examined here, the ERA-I (and TropFlux) estimates are generally best at tracking wind stress based on the TAO/TRITON wind observations and best at resolving the observed wind events. But ERA-I still has substantial offsets from TAO/TRITON (rms offset = 38% of TAO/TRITON standard deviation), including an easterly bias relative to TAO/TRITON in each year since 2004. This recent tendency for easterly bias followed an earlier period in which the offsets were mainly of opposite sign. As a result, the study-period trend in equatorial Pacific zonal wind estimated by ERA-I, and its change in mean over the first to second half of the study period, is substantially different (factor of 2 for the 1992–2011 period) from the one observed by TAO.

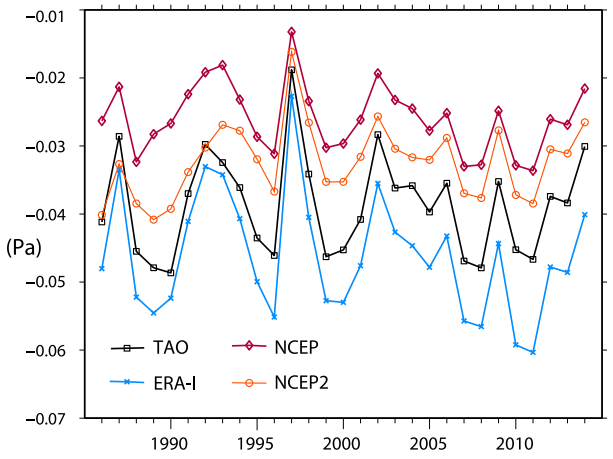

FIG. 7. Yearly averaged wind stress across the equatorial Pacific (2°S–2°N, 137°E–95°W) based on the available TAO/TRITON wind observations (black). ERA-I (blue), NCEP (purple), and NCEP2 (orange) have been subsampled based on the available buoy observations.

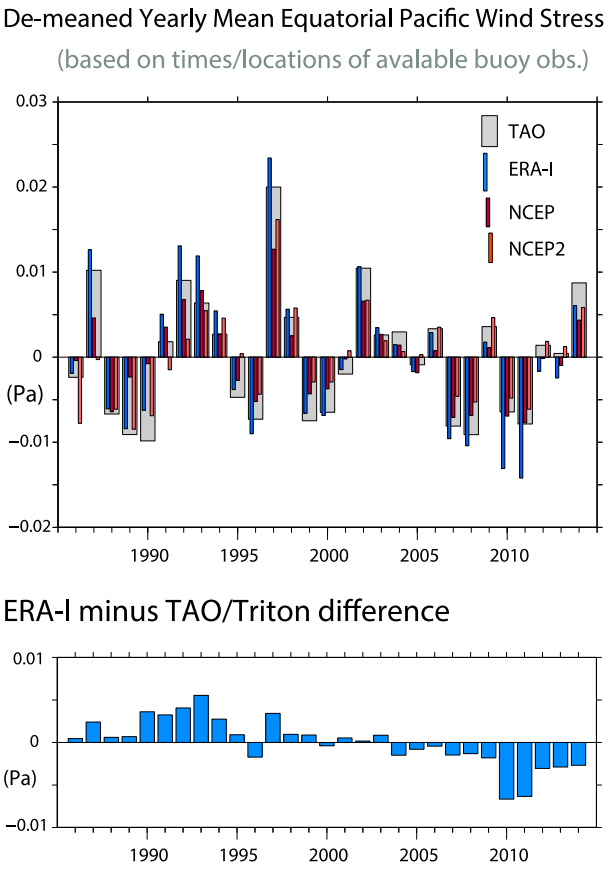

FIG. 8. (top) Demeaned yearly averaged wind stress across the equatorial Pacific (2°S–2°N, 137°E–95°W) based on the available TAO/TRITON wind observations: TAO (gray), ERA-1 (blue), NCEP (red), and NECP2 (orange). (bottom) Difference between the ERA-I- and TAO/TRITON-based results.

5. Forced-OGCM simulations of end-of-year Niño-3.4 SSTA conditions

End-of-year ENSO SSTA conditions can be affected by many factors, including ocean initial conditions, surface heat fluxes (which depend, in part, on the wind speed), and wind stress. Here, we take a broad-scale look at the results of using just wind–wind stress to force an OGCM. Following the OGCM-simulation procedure described above, we have used the wind stress estimates produced by each numerical weather reanalysis to hindcast ocean conditions in each year from 1992 to 2011. Each annual hindcast starts in January from an initial condition of zero ocean anomaly, and the full reanalysis wind stress field product (without any coverage gaps) is used to continually force the ocean model. We have also hindcast each year in the same manner, except using the available TAO/TRITON wind observations on their own. We have tabulated the end-of-year (OND) Niño-3.4 SSTA averages from each year and each set of hindcasts. The model results are compared with observations in Figs. 9 and 10, where the observed end-of-year (OND) Niño-3.4 SSTA conditions are plotted with open bars and model hindcast results are overlaid using wider solid bars. Comparison of the fidelity of the SSTAs forced by the different wind stresses permits an independent evaluation of the quality of the different wind products.

The differences between the observed end-of-year SSTAs and those forced by applying the reanalysis wind stress estimates have largely the same character as the TAO/TRITON-reanalysis wind stress offsets discussed above. For example, the year-to-year variability in the net wind stress estimated by NCEP and NCEP2 is much lower (~30%) than that based on TAO/TRITON. Correspondingly, when the NCEP and NCEP2 reanalysis products are applied to the model, they produce an inadequate amount of year-to-year variability in Niño-3.4 SSTAs; the observed standard deviation of OND-averaged Niño-3.4 SSTAs is 1.2°C, whereas the NCEP-based (NCEP2-based) hindcast reproduces a value of only 0.60°C (0.68°C). Consequently, the rmse between hindcast and observed Niño-3.4 values is largest (0.70° and 0.72°C) for these two (NCEP and NCEP2) cases.

The ERA-I results produce about the right amount of total Niño-3.4 variability, but a substantial amount of this is from a spurious trend that is not seen in the SSTA observations. There are a few years in which ERA-I produces a more accurate end-of-year Niño-3.4 value than TAO/TRITON (e.g., in 1994 and 2010), but the overall character of the ERA-I hindcast error (Fig. 10, bottom) suggests that these couple of good years

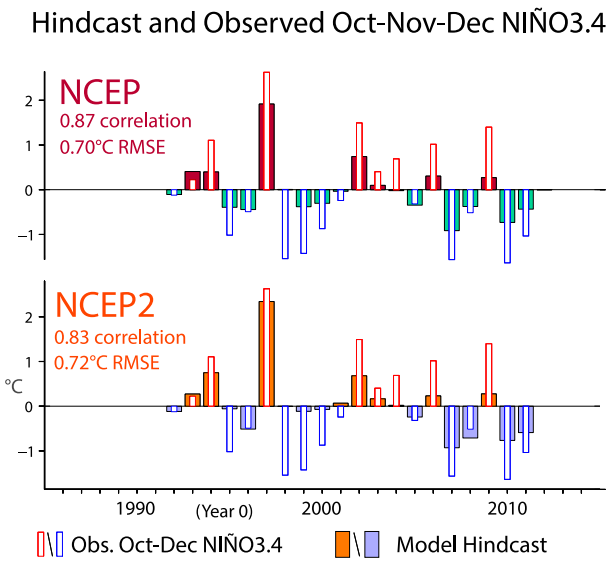

FIG. 9. Observed (thin bars) and hindcast (thicker color-filled bars) OND-averaged Niño-3.4 SSTAs, period 1992–2011. The hindcasts are forced with wind stress from (top) NCEP and (bottom) NCEP2 reanalysis data, respectively. Different colors are used for positive and negative values in each panel.

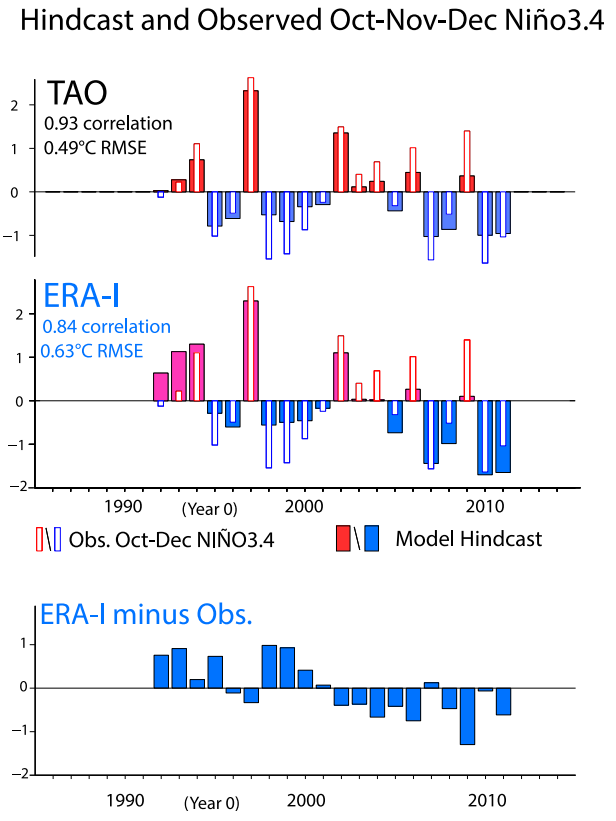

FIG. 10. Observed (thin bars) and hindcast (thicker colored bars) OND-averaged Niño-3.4 SSTAs (°C) forced with wind stress from (top) TAO wind observations and (middle) ERA-I data, respectively. (bottom) The difference between the ERA-I-based result and observed Niño-3.4 SSTAs. Different colors are used for positive and negative values in (top),(bottom).

misleadingly benefit from the unrealistic trendlike bias that is present in the ERA-I dataset. The ERA-I hindcast nonetheless produces a better rmse (0.63°C) than NCEP (0.70°C) or NCEP2 (0.72°C).

Overall, the most accurate hindcast is produced by applying the TAO/TRITON wind stress to the model. We have confirmed that this result holds even if the reanalysis-based hindcasts are rerun after sampling them according to TAO/TRITON coverage [e.g., when the ERA-I hindcast is modified to include the buoy-coverage gaps in its applied wind forcing, it yields observation comparison statistics (rmse = 0.62°C and correlation of 0.84) almost identical to the original hindcast; evidently the reanalysis does not fill these gaps in a manner that improves hindcast accuracy]. In the TAO/TRITON case, the rmse of 0.49°C is less than half of the target OND Niño-3.4 standard deviation, and the correlation is high (0.93). This result demonstrates that OGCM simulations forced with TAO/TRITON observations on their own reproduce observed SSTAs accurately enough to be a useful tool for helping to understand the observed SSTAs.

We take a closer look at the relationship between the applied wind stress and forced model Niño-3.4 behavior in Figs. 11–13, which show, for the 2011 case, hindcasts based on NCEP, NCEP2, and ERA-I (Figs. 11 and 12), as well as TAO/TRITON hindcasts (Fig. 12), and the respective wind stresses at selected TAO sites (Fig. 13). The year 2011 was a La Niña year that is among the ENSO-event years that are more accurately reproduced by the model.

The TAO-based hindcast accurately reproduces the observed Niño-3.4 behavior in this case, suggesting both that zonal wind stress provided the dominant driver for the observed changes in Niño-3.4 region SSTAs this year and that the TAO/TRITON wind observations provide this information with a useful degree of accuracy and resolution. The reanalysis-based hindcasts each produce much larger errors than the TAO/TRITON result. The NCEP and NCEP2 hindcasts fail to produce as much Niño-3.4 cooling as was observed over the end of the year. We attribute this error largely to the fact that the NCEP and NCEP2 wind stress estimates (shown at selected sites below) substantially underrepresent the amplitude of the easterly wind events that occurred in the eastern equatorial Pacific in the several months prior to this time. Such easterly wind events have been shown recently to play a substantial role in the onset and development of La Niña SSTA anomalies (Chiodi and Harrison 2015).

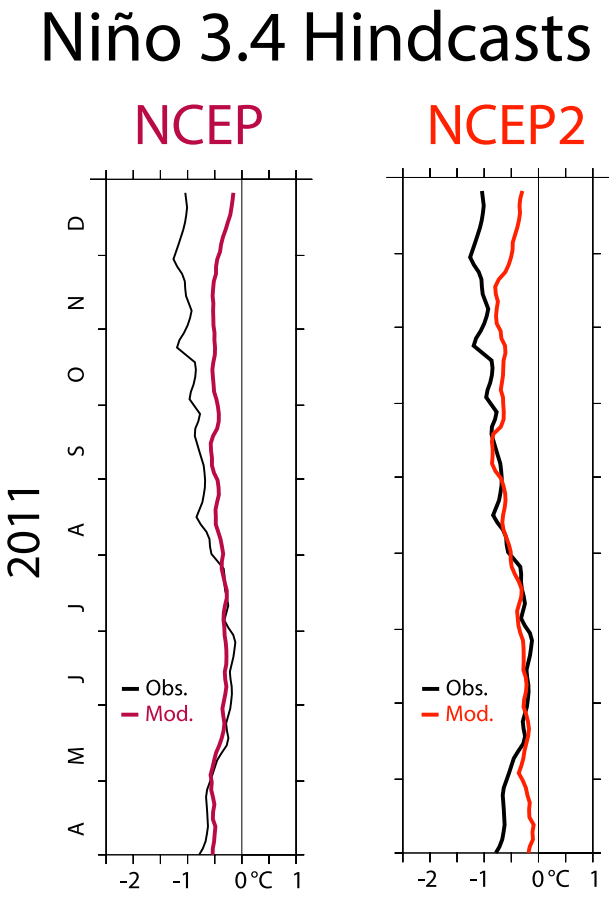

FIG. 11. Hindcast of April–December 2011 Niño-3.4 SSTAs based on the (left) NCEP and (right) NCEP2 wind stress estimates.

The ERA-I-based 2011 Niño-3.4 hindcast shows a consistent cool bias compared to observations, which can be attributed to the easterly offsets in the ERA-I wind stress estimates with respect to TAO/TRITON. In fact, we find that when we adjust the ERA-I estimates by TAO/TRITON (by adding the 2011 offset value shown in Fig. 8 (bottom) to the applied ERA-I wind stress), we basically recover the quantitatively correct TAO/TRITON-based result (Fig. 12, right). Immediate improvement of ERA-I is available by adjusting it by TAO/TRITON.

6. Discussion and conclusions

The TAO/TRITON buoy array was designed in the 1980s and fully deployed across the tropical Pacific in 1994 as a minimal system capable of accurately measuring the main elements of the equatorial Pacific wind behavior associated with the seasonal cycle and ENSO events. A key element of the array design is that the distances between the buoys roughly match the respective meridional and zonal coherence length scales of the observed winds (Harrison and Luther 1990). This enables wind stress fields to be synthesized from TAO/TRITON observations with reasonably high confidence when (nearly) all buoys are reporting. Having been deployed now for over two decades, we find it timely to reexamine the impacts that the wind stress information provided by TAO/TRITON has on our ability to understand the ENSO SSTA behavior seen over this time.

Results here demonstrate, based on examples of a moderate El Niño (2002), strong El Niño (1997), and La Niña (2011) year, that forced ocean model simulation of the detailed development of ENSO SSTAs is feasible with the accurate knowledge of equatorial near-surface wind behavior provided by TAO/TRITON buoy wind observations. The detailed development of ENSO SSTAs (including 2002 and, more often, 1997) has been looked at in many previous ocean model hindcast studies (e.g., Harrison et al. 1990; Auad et al. 2001; Vialard et al. 2001; Vecchi and Harrison 2003, 2006). However, it has not been demonstrated, until now, that observed SSTA development can be accurately reproduced in a model when forced by the TAO/TRITON wind observations on their own.

When we synthesize a wind stress field from the available TAO/TRITON wind observations and use it to force the model over each of the 20 years (1992–2011) with mostly complete (>60%) TAO/TRITON coverage along the equator, the resulting simulations of SSTAs capture most of the observed end-of-year Niño-3.4 SSTA behavior seen over this time (rmse = 0.49°C; correlation = 0.93). It bears noting that this rmse is less than half of the observed OND-averaged Niño-3.4 standard deviation. Thus, the wind observations from TAO/TRITON on their own, along with a sufficiently capable ocean model, provide a basis for understanding most (~85%, by the traditional correlation-squared metric) of the observed end-of-year region-averaged Niño-3.4 variability.

Additional experiments that omit the buoys west of 180° longitude confirm earlier observing system experiments (e.g., Harrison 1989) that showed that accurate knowledge of the winds across the entire equatorial Pacific basin is critical to our ability to understand the development and growth of SSTAs over the waveguide during ENSO events (about half the Niño-3.4 SSTA signal is lost in 2002 without accurate knowledge of the wind stress anomaly over the western Pacific, which we show to be provided by TRITON). The eminent loss of the TRITON buoys motivates the question of how accurate we can expect our knowledge of western equatorial Pacific wind behavior to be without them. Repeating an analysis like ours with reanalyses and/or

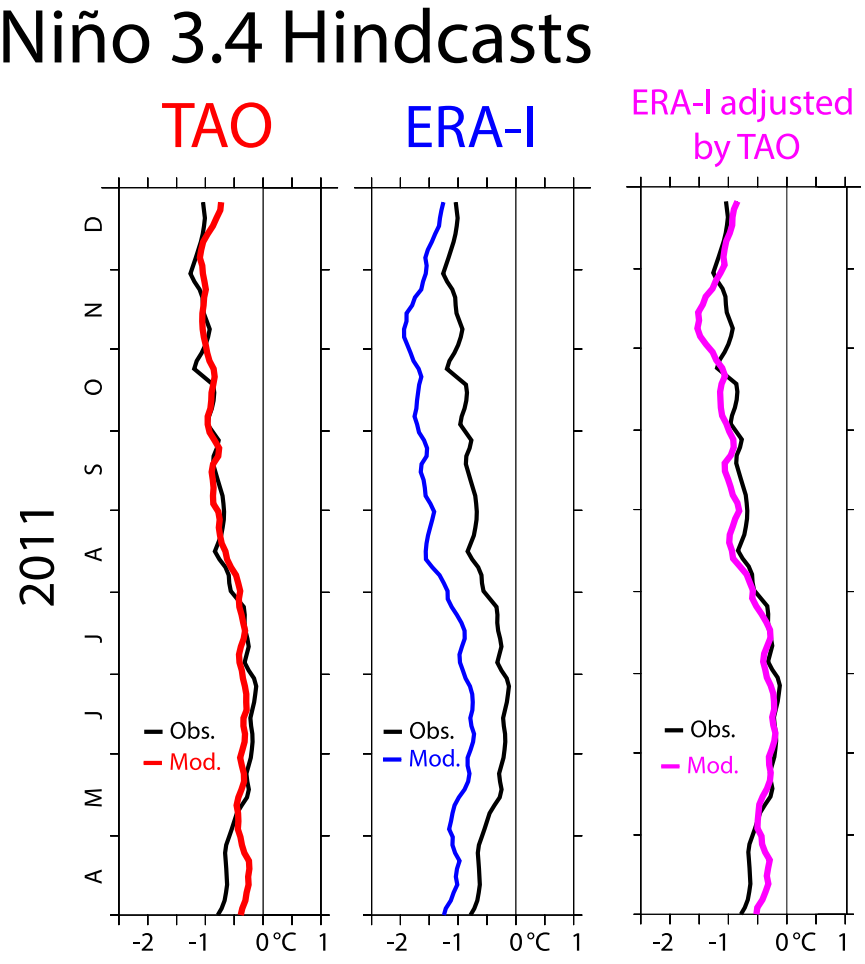

FIG. 12. Hindcast of April to December 2011 Niño-3.4 SSTAs based on (left) TAO/TRITON and (center) ERA-I stress values. (right) The result of first adjusting ERA-I stress estimates to TAO/TRITON.

satellite-based winds that have been produced/calibrated without access to the buoy observations (or other products that have accessed the buoy observations) offers a means to address this question, but we are not aware of any such products, and it is beyond the scope of this study to produce one. More work is needed to reliably address this question.

When we repeat the model runs as before, except using the full resolution wind stress products from the reanalyses (which do have access to TAO/TRITON), we find serious deficiencies in the results. The NCEP and NCEP2 reanalysis products have unrealistically low wind event amplitudes and correspondingly weak cumulative wind stress anomalies that prevent these products from driving sufficient amounts of year-to-year SSTA variability in the ocean model; the modeled standard deviation of OND-average Niño-3.4 SSTAs is 0.61°C (0.70°C) for the NCEP (NCEP2) case, whereas the observed value is 1.2°C over the 1992–2011 study period. These results confirm previous findings that the NCEP reanalysis product is deficient compared to in situ observations in this respect (cf. Wittenberg 2004) and also show that this problem extends to the NCEP2 reanalysis product.

The deficiencies of the ERA-I wind stress product have a different character over the tropical Pacific than NCEP's. Most notably, the ERA-I wind stress tends to have a westerly bias relative to TAO/TRITON in the pre-2000 part of the study period and an easterly bias in the latter half of the study period. As a result, the 20-yr trend in ERA-I over 1992–2011 has a spurious component that causes it to exceed the corresponding TAO/TRITON result by a factor of 2. In the 2011 case, the recent-period easterly bias in ERA-I produces a cool bias of about −0.5°C in the simulated end-of-year Niño-3.4 value. However, ERA-I has appropriate levels of variability, and a substantially more accurate result can be obtained by adjusting ERA-I by TAO/TRITON.

It bears emphasizing that each reanalysis has the TAO/TRITON data available for assimilation, but the

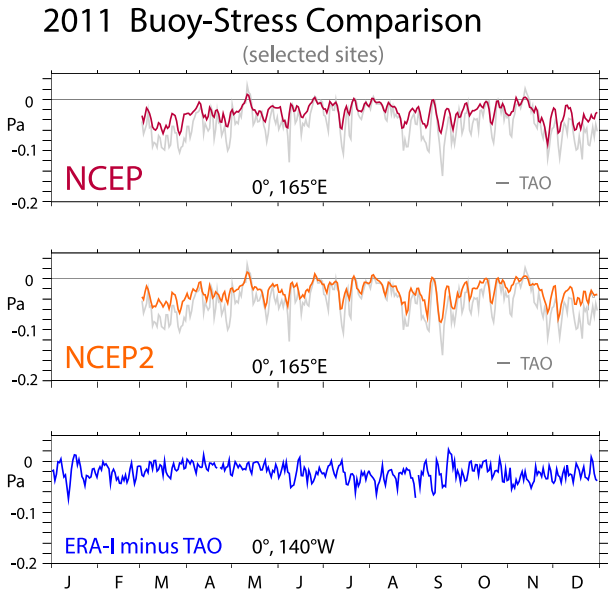

FIG. 13. Comparison of (top) NCEP (red) and (middle) NCEP2 (orange) monthly stress estimates with TAO/TRITON (gray) at the 0°–165°E buoy site. The easterly wind surges observed here in 2011 by TAO/TRITON are underrepresented in NCEP and NCEP2. (bottom) ERA-I minus TAO/TRITON wind stress difference at 0°–140°W, showing that ERA-I usually overestimates the strength of the trade winds during this time.

integrity of the assimilation system has been shown to be less than optimal by the results described herein. The difficulties involved in compiling and properly cataloging the vast quantities of in situ data and metadata available from the various constituent platforms (e.g., moored buoys, volunteer observing ships, drifting buoys, research–service cruises, etc.) are substantial. Successful efforts to ensure that the observations are made publicly available using common, agreed upon, and appropriate data and metadata formats across the various platforms may be necessary to improve the effectiveness of the reanalysis assimilation techniques, which often rely upon externally available observation compilations (e.g., ICOADS; Woodruff et al. 2011).

Despite the successes of the TAO/TRITON hindcasts compared to the reanalysis hindcasts, they remain imperfect. Particularly, the TAO/TRITON hindcasts often fail to reproduce the full amplitude of the observed Niño-3.4 anomalies. This is the case, for example, in 2009, which was simulated with weaker-than-observed amplitude despite having observed Niño-3.4 amplitudes close to those seen in 2002 (which was simulated accurately). Errors such as these may be due to a number of factors, including contributions from surface heat flux variability and initial ocean conditions not represented in our ocean model parameterization, as well as model errors. Also, since TAO/TRITON coverage is not perfect in any of these years, it is reasonable to expect that some of the missing variance can be attributed to the missing wind observations; without complete and accurate knowledge of the winds over the waveguide, it is difficult to gauge the importance of other factors.

It bears noting that the trend in equatorial Pacific wind stress over this period has garnered a substantial amount of attention recently for its possible role in explaining the variability seen in various aspects of Earth's climate, including decadal-time-scale sea surface height changes in the western tropical Pacific (Han et al. 2014; McGregor et al. 2012) and the so-called global warming hiatus, which refers to the relatively rapid rise and then flattening of the global surface temperature trend in recent decades (England et al. 2014; McGregor et al. 2014). The estimation of the equatorial Pacific wind stress trend based specifically on the ERA-I product has played a prominent role in many of these studies [e.g., England et al. (2014) apply ERA-I-produced tropical Pacific wind stress to the coupled models that they use to estimate its effect on global surface temperature]. Our results provide a timely reminder that, even though numerical weather model reanalyses assimilate the available observations, they may still exhibit substantially spurious behavior. The observed trend in equatorial Pacific wind stress over the 1992–2011 period is not given accurately by ERA-I. Though deficient along the waveguide in many other respects, the NCEP and NCEP2 reanalysis products yield 1992–2011 zonal wind stress trends that are much more consistent with the observations than ERA-I.

The reanalysis wind products we have examined here are the ones we have seen most commonly used in the recently published studies of the tropical Pacific coupled air–sea system. Our examination, however, is not exhaustive in that there are other reanalysis (as well as some scatterometer-based) wind products currently available that have not yet been as heavily used in such studies [e.g., NOAA's Climate Forecast System Reanalysis (CFSR), NASA's Modern-Era Retrospective Analysis for Research and Applications (MERRA), and the Japanese 55-year Reanalysis (JRA-55)]. We expect the methodology developed here to be also useful for analyzing the quality of the equatorial wind/wind stress products made available by these other products but have not yet similarly examined the effective integrity of the TAO/TRITON wind assimilation (or calibration) procedures used in these other cases. What has been demonstrated here is that the reanalyses we have considered would be much more useful for ENSO and tropical Pacific climate change study if they would more effectively assimilate the TAO/TRITON observations.

The ongoing effort to design and deploy a next-generation tropical Pacific observing system that is

capable of advancing ENSO science and forecasting ability will likely involve consideration of changes in the configuration of the tropical Pacific moored buoy array. The buoy array in place currently was designed to be minimally redundant based on the zonal (~15° longitude) and meridional (2°–3° latitude) coherence length scales determined from the equatorial Pacific surface wind observations available prior to the deployment of the array. Given the demonstrated success of the current configuration, we suggest that this design principle will serve as a useful guideline for assessing the capability of possible alternative configurations to measure spatial variations in the wind over the equatorial Pacific.

The successes we describe in using TAO/TRITON winds to simulate end-of-year Niño-3.4 conditions in an ocean model remind us of the dominant importance that equatorial zonal winds have on ENSO SSTA development but do not preclude the importance of other factors. There are also other phenomena widely considered to be important aspects of the anomaly state of the tropical Pacific, such as the basin-scale eastward spread of deep atmospheric convection activity that is seen during major El Niño events. Improving our understanding of these aspects may depend upon information from buoys outside of the heart of the waveguide, but our work does not address these issues. What is clear is that maintaining and improving upon (e.g., reducing the number of buoy dropouts) the wind observations currently made available by a tropical Pacific buoy array is one way to progress our understanding of the processes that control the development of equatorial Pacific SSTAs during ENSO events.

Acknowledgments. The authors thank the three anonymous reviewers for their time and helpful comments, as well as P. Poli for helpful conversation. This publication is partially funded by the Joint Institute for the Study of the Atmosphere and Ocean (JISAO) under National Oceanic and Atmospheric Administration (NOAA) Cooperative Agreement NA10OAR4320148 and by support from the Climate Observations Division of the NOAA Climate Program Office (FundRef number 100007298) as well as from NOAA's Pacific Marine Environmental Laboratory.

REFERENCES

Atlas, R., R. N. Hoffman, J. Ardizzone, S. M. Leidner, J. C. Jusem, D. K. Smith, and D. Gombos, 2011: A cross-calibrated, multiplatform ocean surface wind velocity product for meteorological and oceanographic applications. *Bull. Amer. Meteor. Soc.*, **92**, 157–174, doi:10.1175/2010BAMS2946.1.

Auad, G., A. J. Miller, J. O. Roads, and D. Cayan, 2001: Pacific Ocean wind stress and surface heat flux anomalies from NCEP reanalysis and observations: Cross-statistics and ocean model responses. *J. Geophys. Res.*, **106**, 22 249–22 265, doi:10.1029/2000JC000264.

Bryan, K., 1969: A numerical method for the study of the circulation of the world ocean. *J. Comput. Phys.*, **4**, 347–376, doi:10.1016/0021-9991(69)90004-7.

Chen, D., and Coauthors, 2015: Strong influence of westerly wind bursts on El Niño diversity. *Nat. Geosci.*, **8**, 339–345, doi:10.1038/ngeo2399.

Chiodi, A. M., and D. E. Harrison, 2015: Equatorial Pacific easterly wind surges and the onset of La Niña events. *J. Climate*, **28**, 776–792, doi:10.1175/JCLI-D-14-00227.1.

——, ——, and G. A. Vecchi, 2014: Subseasonal atmospheric variability and El Niño waveguide warming: Observed effects of the Madden–Julian oscillation and westerly wind events. *J. Climate*, **27**, 3619–3642, doi:10.1175/JCLI-D-13-00547.1.

Cox, M. D., 1984: A primitive equation, 3-dimensional model of the ocean. GFDL Ocean Group Tech. Rep. 1, 143 pp.

Cronin, M. F., C. W. Fairall, and M. J. McPhaden, 2006: An assessment of buoy-derived and numerical weather prediction surface heat fluxes in the tropical Pacific. *J. Geophys. Res.*, **111**, C06038, doi:10.1029/2005JC003324.

Dee, D. P., and Coauthors, 2011: The ERA-Interim reanalysis: Configuration and performance of the data assimilation system. *Quart. J. Roy. Meteor. Soc.*, **137**, 553–597, doi:10.1002/qj.828.

ECMWF, 2011: ERA Interim, daily. ECMWF, accessed 1 August 2015. [Available online at http://apps.ecmwf.int/datasets/data/interim-full-daily.]

England, M. H., and Coauthors, 2014: Recent intensification of wind-driven circulation in the Pacific and the ongoing warming hiatus. *Nat. Climate Change*, **4**, 222–227, doi:10.1038/nclimate2106.

Fairall, C. W., E. F. Bradley, J. E. Hare, A. A. Grachev, and J. B. Edson, 2003: Bulk parameterization of air–sea fluxes: Updates and verification for the COARE algorithm. *J. Climate*, **16**, 571–591, doi:10.1175/1520-0442(2003)016<0571:BPOASF>2.0.CO;2.

Flato, G., and Coauthors, 2013: Evaluation of climate models. *Climate Change 2013: The Physical Science Basis*, T. F. Stocker et al., Eds., Cambridge University Press, 741–866, doi:10.1017/CBO9781107415324.020.

Gnanadesikan, A., and Coauthors, 2006: GFDL's CM2 global coupled climate models. Part II: The baseline ocean simulation. *J. Climate*, **19**, 675–697, doi:10.1175/JCLI3630.1.

Griffies, S. M., M. J. Harrison, R. C. Pacanowski, and A. Rosati, 2003: A technical guide to MOM4. GFDL Ocean Group Tech. Rep. 5, 295 pp.

Han, W., and Coauthors, 2014: Intensification of decadal and multi-decadal sea level variability in the western tropical Pacific during recent decades. *Climate Dyn.*, **43**, 1357–1379, doi:10.1007/s00382-013-1951-1.

Harrison, D. E., 1989: On climatological monthly mean wind stress and wind stress curl fields over the World Ocean. *J. Climate*, **2**, 57–70, doi:10.1175/1520-0442(1989)002<0057:OCMMWS>2.0.CO;2.

——, 1991: Equatorial sea surface temperature sensitivity to net surface heat flux: Some ocean circulation model results. *J. Climate*, **4**, 539–549, doi:10.1175/1520-0442(1991)004<0539:ESSTST>2.0.CO;2.

——, and D. S. Luther, 1990: Surface winds from tropical Pacific islands—Climatological statistics. *J. Climate*, **3**, 251–271, doi:10.1175/1520-0442(1990)003<0251:SWFTPI>2.0.CO;2.

——, and A. M. Chiodi, 2009: Pre- and post-1997/98 westerly wind events and equatorial Pacific cold tongue warming. *J. Climate*, **22**, 568–581, doi:10.1175/2008JCLI2270.1.

——, and ——, 2015: Multi-decadal variability and trends in the El Niño–Southern Oscillation and tropical Pacific fisheries implications. *Deep Sea Res. II*, **113**, 9–21, doi:10.1016/j.dsr2.2013.12.020.

——, B. S. Giese, and E. S. Sarachik, 1990: Mechanisms of SST change in the equatorial waveguide during the 1982–83 ENSO. *J. Climate*, **3**, 173–188, doi:10.1175/1520-0442(1990)003<0173:MOSCIT>2.0.CO;2.

——, A. M. Chiodi, and G. A. Vecchi, 2009: Effects of surface forcing on the seasonal cycle of the eastern equatorial Pacific. *J. Mar. Res.*, **67**, 701–729, doi:10.1357/002224009792006179.

Kalnay, E., and Coauthors, 1996: The NCEP/NCAR 40-Year Reanalysis Project. *Bull. Amer. Meteor. Soc.*, **77**, 437–471, doi:10.1175/1520-0477(1996)077<0437:TNYRP>2.0.CO;2.

Kanamitsu, M., W. Ebisuzaki, J. Woollen, S.-K. Yang, J. J. Hnilo, M. Fiorino, and G. L. Potter, 2002: NCEP–DOE AMIP-II reanalysis (R-2). *Bull. Amer. Meteor. Soc.*, **83**, 1631–1643, doi:10.1175/BAMS-83-11-1631.

Kumar, A., and Z.-Z. Hu, 2012: Uncertainty in the ocean–atmosphere feedbacks associated with ENSO in the reanalysis products. *Climate Dyn.*, **39**, 575–588, doi:10.1007/s00382-011-1104-3.

Large, W. G., and S. Pond, 1981: Open ocean momentum flux measurements in moderate to strong winds. *J. Phys. Oceanogr.*, **11**, 324–336, doi:10.1175/1520-0485(1981)011<0324:OOMFMI>2.0.CO;2.

Legler, D. M., and J. J. O'Brien, 1988: Tropical Pacific wind stress analysis for TOGA. *Time Series of Ocean Measurements*, Intergovernmental Oceanographic Commission Tech. Series 33, Vol. 4, United Nations Educational, Scientific and Cultural Organization, 11–17. [Available online at http://ioc-unesco.org/index.php?option=com_oe&task=viewDocumentRecord&docID=893.]

McGregor, S., A. Sen Gupta, and M. H. England, 2012: Constraining wind stress products with sea surface height observations and implications for Pacific Ocean sea level trend attribution. *J. Climate*, **25**, 8164–8176, doi:10.1175/JCLI-D-12-00105.1.

——, A. Timmerman, M. F. Stuecker, M. H. England, M. Merrifield, F.-F. Jin, and Y. Chikamoto, 2014: Recent Walker circulation strengthening and Pacific cooling amplified by Atlantic warming. *Nat. Climate Change*, **4**, 888–892, doi:10.1038/nclimate2330.

McPhaden, M. J., and Coauthors, 2010: The global tropical moored buoy array. *Proc. OceanObs'09: Sustained Ocean Observations and Information for Society Conf.*, Venice, Italy, European Space Agency, 61, doi:10.5270/OceanObs09.cwp.61.

Menkes, C. E., M. Lengaigne, J. Vialard, M. Puy, P. Marchesiello, S. Cravatte, and G. Cambon, 2014: About the role of westerly wind events in the possible development of an El Niño in 2014. *Geophys. Res. Lett.*, **41**, 6476–6483, doi:10.1002/2014GL061186.

Min, Q., J. Su, R. Zhang, and X. Rong, 2015: What hindered the El Niño pattern in 2014? *Geophys. Res. Lett.*, **42**, 6762–6770, doi:10.1002/2015GL064899.

National Institute of Oceanography and IPSL, 2012: TropFlux: Air–sea heat and momentum fluxes for the global tropical oceans. Council of Scientific and Industrial Research–National Institute of Oceanography and IPSL, accessed 1 August 2015. [Available online at http://www.incois.gov.in/tropflux_datasets/data/daily/taux.]

NCEP, 1996: NCEP/NCAR Reanalysis 1. NOAA/OAR/ESRL Physical Sciences Division, accessed 1 August 2015. [Available online at http://www.esrl.noaa.gov/psd/data/gridded/data.ncep.reanalysis.html.]

——, 2002: NCEP–DOE Reanalysis 2. NOAA/OAR/ESRL Physical Sciences Division, accessed 1 August 2015. [Available online at http://www.esrl.noaa.gov/psd/data/gridded/data.ncep.reanalysis2.html.]

NOAA, 2002: NOAA optimal interpolation sea surface temperature, version 2. NOAA/OAR/ESRL Physical Sciences Division, accessed 1 August 2015. [Available online at http://www.esrl.noaa.gov/psd/data/gridded/data.noaa.oisst.v2.html.]

Philander, S. G. H., and A. D. Siegel, 1985: Simulation of El Niño of 1982–83. *Coupled Ocean–Atmosphere Models*, J. C. J. Nihoul, Ed., Elsevier, 517–541.

Praveen Kumar, B., J. Vialard, M. Lengaigne, V. S. N. Murty, M. J. McPhaden, M. F. Cronin, F. Pinsard, and K. Gopala Reddy, 2013: TropFlux wind stresses over the tropical oceans: Evaluation and comparison with other products. *Climate Dyn.*, **40**, 2049–2071, doi:10.1007/s00382-012-1455-4.

Reynolds, R. W., N. A. Rayner, T. M. Smith, D. C. Stokes, and W. Wang, 2002: An improved in situ and satellite SST analysis for climate. *J. Climate*, **15**, 1609–1625, doi:10.1175/1520-0442(2002)015<1609:AIISAS>2.0.CO;2.

Semtner, A. J., Jr., 1974: An oceanic general circulation model with bottom topography. Dept. of Meteorology, University of California, Los Angeles, Tech. Rep. 9, 99 pp.

Serra, Y. L., M. F. Cronin, and G. N. Kiladis, 2007: Sub-seasonal variance of surface meteorological parameters in buoy observations and reanalyses. *Geophys. Res. Lett.*, **34**, L12708, doi:10.1029/2007GL029506.

Smith, S. R., D. M. Legler, and K. V. Verzone, 2001: Quantifying uncertainties in NCEP reanalyses using high-quality research vessel observations. *J. Climate*, **14**, 4062–4072, doi:10.1175/1520-0442(2001)014<4062:QUINRU>2.0.CO;2.

Stevenson, S., B. Fox-Kemper, M. Jochum, B. Rajagopalan, and S. G. Yeager, 2010: ENSO model validation using wavelet probability analysis. *J. Climate*, **23**, 5540–5547, doi:10.1175/2010JCLI3609.1.

TAO Project Office, 2000: Tropical Atmosphere Ocean/Triangle Trans-Ocean Buoy Network. NOAA/PMEL, accessed 1 August 2015. [Available online at http://www.pmel.noaa.gov/tao/data_deliv/deliv.html.]

Vecchi, G. A., and D. E. Harrison, 2003: On the termination of the 2002–03 El Niño event. *Geophys. Res. Lett.*, **30**, 1964, doi:10.1029/2003GL017564.

——, and ——, 2006: The termination of the 1997–98 El Niño. Part I: Mechanisms of oceanic change. *J. Climate*, **19**, 2633–2646, doi:10.1175/JCLI3776.1.

Vialard, J., C. Menkes, J.-P. Boulanger, P. Delecluse, E. Guilyardi, M. J. McPhaden, and G. Madec, 2001: A model study of oceanic mechanisms affecting equatorial Pacific sea surface temperature during the 1997–98 El Niño. *J. Phys. Oceanogr.*, **31**, 1649–1675, doi:10.1175/1520-0485(2001)031<1649:AMSOOM>2.0.CO;2.

Wittenberg, A. T., 2004: Extended wind stress analyses for ENSO. *J. Climate*, **17**, 2526–2540, doi:10.1175/1520-0442(2004)017<2526:EWSAFE>2.0.CO;2.

——, 2009: Are historical records sufficient to constrain ENSO simulations? *Geophys. Res. Lett.*, **36**, L12702, doi:10.1029/2009GL038710.

Woodruff, S. D., and Coauthors, 2011: ICOADS release 2.5: Extensions and enhancements to the surface marine meteorological archive. *Int. J. Climatol.*, **31**, 951–967, doi:10.1002/joc.2103.

Zhang, H.-M., J. J. Bates, and R. W. Reynolds, 2006: Assessment of composite global sampling: Sea surface wind speed. *Geophys. Res. Lett.*, **33**, L17714, doi:10.1029/2006GL027086.